Applied Physics Letters

Out-of-plane ferroelectricity and multiferroicity in elemental bilayer phosphorene, arsenene, and antimonene

Cite as: Appl. Phys. Lett. **118**, 012905 (2021); https://doi.org/10.1063/5.0032790
Submitted: 11 October 2020 • Accepted: 17 December 2020 • Published Online: 06 January 2021

Yan Liang, Rongjing Guo, Shiying Shen, et al.

Applied Physics Letters ARTICLE scitation.org/journal/apl

Out-of-plane ferroelectricity and multiferroicity in elemental bilayer phosphorene, arsenene, and antimonene

Cite as: Appl. Phys. Lett. **118**, 012905 (2021); doi: 10.1063/5.0032790
Submitted: 11 October 2020 · Accepted: 17 December 2020 ·
Published Online: 6 January 2021

Yan Liang, Rongjing Guo, Shiying Shen, Baibiao Huang, Ying Dai,[a] and Yandong Ma[a]

AFFILIATIONS

School of Physics, State Key Laboratory of Crystal Materials, Shandong University, Shandanan Str., 27, Jinan 250100, People's Republic of China

[a]Authors to whom correspondence should be addressed: daiy60@sina.com and yandong.ma@sdu.edu.cn

ABSTRACT

Developing out-of-plane ferroelectricity in a two-dimensional (2D) lattice is becoming increasingly important due to its high potential for miniaturized device applications. Current research efforts for 2D out-of-plane ferroelectrics mainly focus on compounds, while 2D elemental material-based ferroelectrics have been rarely explored. Herein, we show first-principles evidence of the existence of out-of-plane ferroelectricity in elemental 2D lattices, bilayer phosphorene, arsenene, and antimonene, which can be easily synthesized in a controllable manner in experiments. Our results reveal that their sizable out-of-plane polarizations are attributed to the charge redistribution caused by the unique stacking pattern. Upon doping holes, bilayer phosphorene and arsenene are shown to be multiferroic, presenting a strong coupling between ferroelectricity and ferromagnetism. Moreover, reversible spin texture induced by ferroelectric switching is achieved in all these three systems. These findings thereby not only broaden the class of 2D out-of-plane ferroelectrics but also enable future multifunctional nanodevice designs.

Ferroelectric materials exhibit a spontaneous polarization that is stable and can be reversed hysteretically in the presence of an external electric field, offering fundamental promise for nonvolatile information technology with the advantage of fast device operation and high storage density.[1,2] In the last few decades, plenty of traditional ferroelectric materials, usually based on complex oxides such as ABO_3 perovskites,[3] $BaBi_2Ta_2O_9$,[4] and $Tl_2Cd_2(SO_4)_3$,[5] were reported, and many of them have found their commercial applications.[6] Meanwhile, with the continuation of device miniaturization, much effort has been made toward realizing ferroelectricity in thin films.[7] Compared with the in-plane ferroelectricity, out-of-plane (OOP) ferroelectricity in thin films is more favorable as most technologies are related to polarizability perpendicular to the plane. The existence of OOP ferroelectricity in thin films is supported by theoretical investigations decades ago,[8,9] but spontaneous electric polarization in ferroelectric oxides usually disappears in experiments as the film is thinned below a critical value around several to tens of nanometers,[10,11] resulting from the effects of surface reconstruction, depolarizing electrostatic field, and electron screening.[11–13]

The recent emergence of graphene provides an unprecedented opportunity for exploring ferroelectric materials with OOP polarization in 2D scale. So far, OOP ferroelectricity has been discovered in many 2D systems. Examples include 2D $MoTe_2$,[14] WTe_2,[15] In_2Se_3,[16] $CuInP_2S_6$,[17] Sc_2CO_2,[18] binary compound multilayers,[19] and so on.[20–23] It is interesting to note that all these reported 2D OOP ferroelectrics are based on the compounds that are composed of two or more elements. To date, 2D elemental material-based OOP ferroelectrics have never been reported despite some work on 2D elemental materials with in-plane ferroelectrics.[24–29] This limitation mainly arises from the fact that the existence of multiple elements with different electronegativities is conventionally considered as a necessary precondition for inducing large ion-displacement dipoles.

In this work, we show that OOP ferroelectricity can exist in 2D elemental materials. Using first-principles calculations, we demonstrate that bilayer phosphorene, arsenene, and antimonene, which exhibit high experimental feasibility, possess intriguing ferroelectricity with a sizeable OOP polarization. The underlying physics for such polarization is related to the charge redistribution induced by unique lattice stacking. In particular for bilayer phosphorene and arsenene, arising from their particular electronic structures, they display multiferroic phases, wherein the ferroelectricity and ferromagnetism are coupled strongly, under proper hole doping. In addition, the spin

textures for all these three systems are reversible in the presence of ferroelectric switching. Our work is useful for the fundamental research in ferroelectrics and multiferroics.

First-principles calculations are performed based on density functional theory as implemented in the Vienna *Ab Initio* Simulation Package (VASP).[30] The generalized gradient approximation (GGA) in the form of Perdew, Burke, and Ernzerhof (PBE)[31] is used to describe the exchange correlation. The PBE-D3 method is employed for taking van der Waals interaction into account.[32] The cutoff energy is set to be 500 eV. A vacuum space larger than 18 Å is employed to eliminate the spurious interactions. Structures are fully relaxed with convergence criteria of 10^{-5} eV and 0.01 eV/Å for energy and forces, respectively. The Brillouin zone integration is sampled with Monkhorst–Pack grids of $9 \times 9 \times 1$. The phonon band calculation is conducted as implemented in the Phonopy code.[33] *Ab initio* molecular dynamic calculations are performed within a $3 \times 3 \times 1$ periodic supercell with canonical (NVT) ensemble at zero pressure and a time step of 1 fs. Curie temperature is estimated by sigmoid fits of the tracked average polarizations in the simulations. Energy barriers of ferroelectric switching are obtained by using the nudged elastic band (NEB) method.[34] The ferroelectric polarization is evaluated by the Berry phase approach.[19,23]

Figure 1(a) shows the crystal structure of bilayer phosphorene, arsenene, and antimonene. The lattice parameters are summarized in Table S1. In these systems, the X (X = P, As, or Sb) atoms from the lower sublattices belonging to both layers overlap directly along the *z* direction, while the X atoms from the upper sublattice of the top monolayer are placed above the center of the honeycomb net formed by the upper sublattice of the bottom layer. They are also denoted by AC′ stacked bilayers in the following investigation. Such a stacking pattern that exhibits the space group *P*3*m*1 (No. 156) will result in the electric polarization, as we will show below. To assess their stabilities, we calculate the phonon band dispersions, which are presented in Figs. 1(b) and S1. Clearly, all phonon modes are positive throughout the whole Brillouin zone, suggesting that all the bilayer systems are dynamically stable. In addition, we investigate the thermal stability of these materials by *ab initio* molecular dynamic simulations. As shown in Fig. S2, the free energies remain almost invariant during the simulation. From the snapshots taken at the end of the simulation, we observe the well-maintained framework as its initial structure, confirming that these elemental materials possess high thermal stability.

In addition, we also investigate the relative stability of this configuration (AC′) with respect to other configurations. Different from bilayer graphene that has only two different relative stacking patterns, there are five typical stacking patterns for these elemental bilayers as they present low-buckled structures, see Fig. 1(c). Our calculations show that the most stable configuration for bilayer arsenene is AC′ [Fig. 1(d)], whereas both bilayer phosphorene and antimonene favor the AC stacking mode. However, the total energy differences between AC′ and AC tacking patterns for bilayer phosphorene and antimonene are only 0.031 and 0.026 eV per unit cell, respectively. These values are similar to the energy difference between experimentally prepared bilayer transition metal dichalcogenides,[23] implying that bilayer phosphorene and antimonene with AC′ stacking also exhibit experimental feasibility. Moreover, we note that the Moire superlattice, formed by a small twisted angle in the van der Waals bilayer,[35,36] can generate a large scale of such local ferroelectric domains.

In the light of the space group *P*3*m*1, neither inversion symmetry nor mirror symmetry in the OOP direction is presented for all these three systems. Apparently, such symmetry broken would allow a net interlayer charge transfer. This is in accordance with the calculated charge density difference. As shown in Fig. 2(a), there is a significant charge transfer from the bottom to top layers, giving rise to a net spontaneous OOP polarization pointing downwards. Figures 2(b) and S3 give their plane averaged electrostatic potentials along the *z* direction. The values of discontinuity (ΔV) between the vacuum levels of the top and bottom layers are found to be 0.05, 0.10, and 0.12 eV, respectively, for bilayer phosphorene, arsenene, and antimonene. It should be noted that the larger the ΔV, the larger the interface dipole and the resultant polarization.[23,37] Importantly, in group-V elemental monolayers crystalized with space group *Pmna*, the in-plane polarization is due to spontaneous lattice distortion with atomic layer bucking.[25] Distinct from this mechanism, nonzero OOP polarization in these hexagonal bilayers is related to the charge redistribution induced by unique lattice stacking.

The existence of electronic polarity does not guarantee ferroelectricity that necessarily requires switchable spontaneous polarization. To verify ferroelectricity in these systems, we propose an interlayer translation polarization reversal pathway [see Fig. 2(c)], which provides an intermediate state and two energetically degenerate states with opposite OOP electric polarizations (states I and II). The intermediate state shows the space group *Abm*2 (No. 39) and no OOP

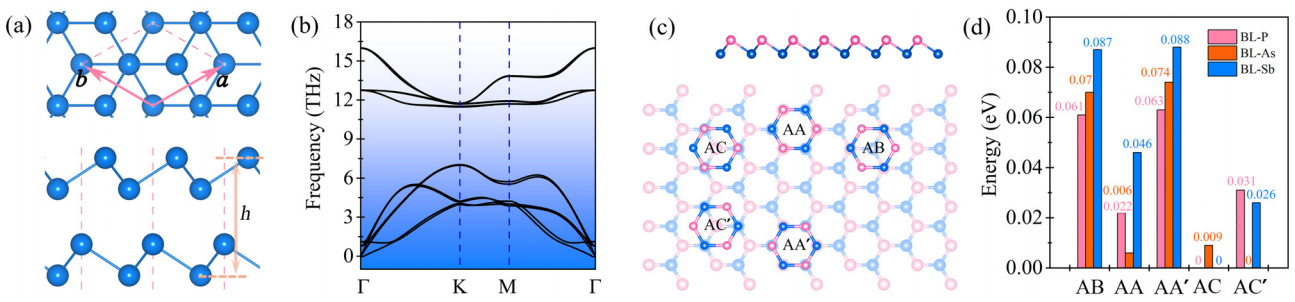

FIG. 1. (a) Top and side views of the crystal structure of bilayer phosphorene, arsenene, and antimonene, where the unit cell is marked with pink dashed lines; the sandy brown double sided arrow defines the effective thickness *h*. (b) Phonon dispersions of bilayer phosphorene. (c) Five typical stacked configurations; the atoms of upper and lower sublattices are distinguished by pink and blue colors, respectively. (d) Total energy differences between the energetically most stable structure and other stacked configurations for bilayer phosphorene, arsenene, and antimonene.

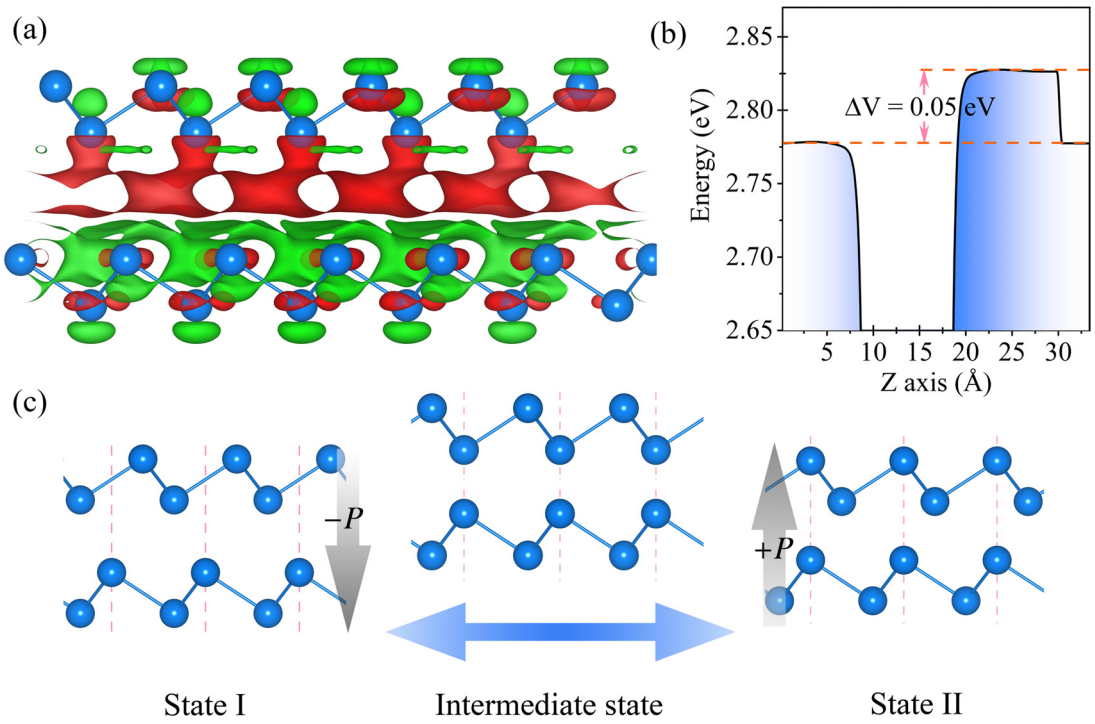

FIG. 2. (a) Charge density difference for bilayer phosphorene; the red and green areas represent electron accumulation and depletion, respectively. (b) Plane averaged electrostatic potential of bilayer phosphorene along the *z* direction. (c) Proposed kinetic polarization reversal pathway.

polarization. It should be noted that such an in-plane sliding transition mechanism is similar to previous van der Waals ferroelectrics,[15,19,23,38,39] which thus is highly plausible. Figure S4 shows the phonon spectra for the intermediate states, from which we can see pronounced negative frequencies around the Γ point. This indicates that the intermediate states are not stable, which would experience spontaneous transformation into the ferroelectric states. To evaluate the possibility and robustness of polarization reversal, the energy barriers from one polarization phase (state I) to another (state II) across the centrosymmetric state are calculated by using the NEB method. We wish to stress that such a transformation is not associated with lattice distortion. As described in Fig. 3(a), the polarization switching should overcome energy barriers of 10, 18, and 38 meV/f.u. for bilayer phosphorene, arsenene, and antimonene, respectively. Such barriers are larger than that of bilayer WTe_2 (~0.6 meV/f.u.),[38] but comparable or lower than that of α-In_2Se_3 (50 meV/f.u.),[40] functionalized bismuth layer (120–548 meV/f.u.),[41] and γ-GeSe (887 meV/f.u.),[42] denoting the feasible and robust ferroelectricity in these systems. We thus can

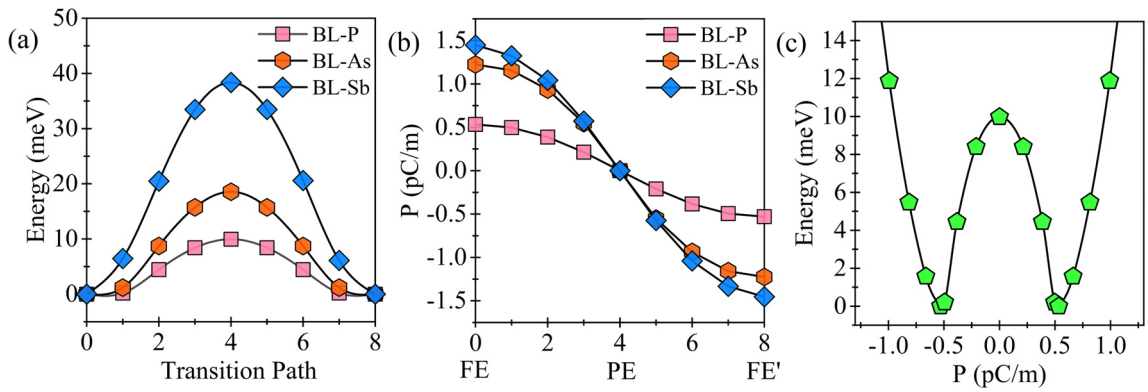

FIG. 3. (a) Energy pathway of ferroelectric switching as a function of step number within the NEB for bilayer phosphorene, arsenene, and antimonene. (b) Variation of total OOP polarization as a function of step number within the NEB for bilayer phosphorene, arsenene, and antimonene. (c) Double-well potential of bilayer phosphorene vs OOP polarization; the energy of the ferroelectric state is set to zero.

conclude that bilayer phosphorene, arsenene, and antimonene are tantalizing 2D ferroelectric materials with OOP polarization.

Having confirmed ferroelectricity in these systems, their intrinsic OOP spontaneous polarizations are evaluated. As shown in Fig. 3(b), the spontaneous vertical polarizations are found to be 0.53, 1.33, and 1.45 pC/m for bilayer phosphorene, arsenene, and antimonene, respectively (corresponding to bulk electric polarization of 0.09, 0.22, and 0.24 μC/cm^2, if we consider the effective thickness). These values are in the order: bilayer phosphorene < bilayer arsenene < bilayer antimonene, agreeing well with the interfacial dipole ΔV in the sequences of bilayer phosphorene (0.05 eV) < bilayer arsenene (0.10 eV) < bilayer antimonene (0.12 eV). Interestingly, the OOP polarizations in these systems are significantly larger than that of the famous bilayer WTe_2 (0.03 μC/cm^2),[38] which means that the experimental detection of the ferroelectricity in these bilayers is totally feasible. Furthermore, we adopt the Landau theory with the polarization P as the order parameter to examine the variation of the total energy.[43] The results are plotted in Figs. 3(c) and S5, from which we can see the typical anharmonic double-well energy curves, again confirming their ferroelectricity. To estimate the stability of their ferroelectricity with temperature, we investigate the Curie temperature. By performing the molecular dynamic simulations,[25] the Curie temperature of bilayer phosphorene, arsenene, and antimonene is estimated to be 472, 456, and 882 K, respectively (Fig. S6), suggesting their practical device applications. It should be noted that the bilayer arsenene has a larger energy barrier than bilayer phosphorene, while its Curie temperature is slightly lower, which may be attributed to the complicated coexistence and mutual effect of ferroelectric and antiferroelectric phases.[25,38]

The band structures of bilayer phosphorene, arsenene, and antimonene are shown in Figs. 4(a) and S7. We can see that they are all indirect bandgap semiconductors. In addition to the semiconducting feature, it is interesting to note that the highest valence band close to the Fermi level exhibits a Mexican-hat-like dispersion for all these three systems. In particular, for bilayer phosphorene, its highest valence band closest to the Fermi level is rather flat. This unique flat character of the band structure gives rise to a sharp density of states (DOS) [see Fig. 4(a)], yielding the so-called Van Hove singularities. It is known that such singularity in DOS below the Fermi level usually causes electronic instability, indicating a great probability for Stoner ferromagnetism induced by appropriate hole doping.[42,44]

To verify the Stoner-type ferromagnetic instability in bilayer phosphorene, we calculate the magnetic moment and the spin polarization energy as a function of hole density. Here, the spin polarization energy is defined as the total energy difference between the nonmagnetic and ferromagnetic phases. As shown in Fig. 4(b), the ferromagnetic state begins to be energetically favorable when the hole concentration is larger than 0.43×10^{14}/cm^2 (0.04 hole/f.u.), and the magnetic moment per hole becomes the largest (1 μ_B/hole) under the hole concentration in the range of $0.54–2.48 \times 10^{14}$/cm^2 (0.05–0.23 hole/f.u.). By further increasing the hole concentration, the magnetic moment per hole is reduced. When increasing the hole density larger than 3.56×10^{14}/cm^2 (0.33 hole/f.u.), bilayer phosphorene returns to be nonmagnetic, as Stoner's criterion $N(E_F)I > 1$ is no longer satisfied. To understand the doping-induced ferromagnetism more clearly, we calculate the Stoner factors $N(E_F)$ and I at the doping concentration of 2.16×10^{14}/cm^2. The obtained values are 5.35 and 0.62, respectively, for $N(E_F)$ and I. According to the Stoner criterion $N(E_F)I > 1$, the itinerant ferromagnetism is induced spontaneously.[42,45] Figure 4(c) shows the band structure of bilayer phosphorene under a hole doping concentration of 2.16×10^{14}/cm^2. It can be seen that its highest spin up valence band near the Fermi level is fully occupied, while the highest spin down valence band near the Fermi level is partially filled, suggesting a half-metallic nature. This half-metallic behavior would allow fully polarized spin transport. Given that doping carriers around 10^{15}/cm^2 can readily be achieved in 2D materials,[46] we are quite confident that the realization of magnetic behaviors in bilayer phosphorene can be achieved. As for bilayer arsenene and antimonene, it is found that doping-induced ferromagnetism can also be achieved in bilayer arsenene under the hole concentration between 2.64 and 6.17×10^{13}/cm^2 (Fig. S8).

From the above discussion, we can see that, under proper hole doping, bilayer phosphorene and arsenene can exhibit ferroelectricity and ferromagnetism simultaneously, achieving the multiferroics. We note that although hole doping will introduce a half-metallic feature, which is previously supposed to quench polarity due to the screening effect. This contra-indicated characteristic is recently challenged by several experimental discoveries, wherein itinerant electrons can even be used to stabilize ferroelectricity in metal.[15,20,47–49] What's more, as mentioned in the previous literature,[20,42,50] free electrons in 2D polar metals with an OOP polarization can be confined within the slab and nonconductive along the OOP direction. Therefore, OOP

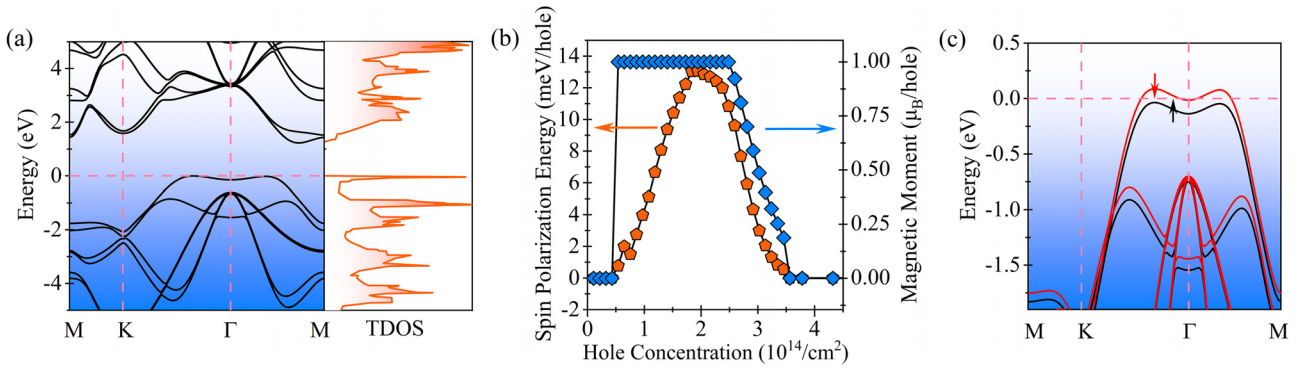

FIG. 4. (a) Band structure and DOS of bilayer phosphorene. (b) Doping dependence of spin polarization energy and the magnetic moment for bilayer phosphorene. (c) Band structure of bilayer phosphorene under the hole doping concentration of 2.16×10^{14}/cm^2 (0.20 hole/f.u.). The Fermi level is set to 0 eV.

ferroelectricity is not likely to be eliminated in these systems. Our calculations also show that after doping, the charge distribution on different layers is still different, which is ascribed to that the unique stacking can maintain the breaking of symmetry and thus favor the robustness of vertical polarizations. It should be noted that the value of electrical polarization may be doping concentration-dependent, which needs to be discussed elaborately elsewhere.

More interestingly, these two ferroic orders are strongly coupled. Due to the charge transfer between the two layers of bilayer phosphorene and arsenene, these opposite layers show significant inequivalent interlayer spin density distributions and, thus, different magnetic moments. Under ferroelectric switching induced by the electric field, the distribution of magnetic moments on these two layers will be switched, making it possible to modulate the magnetization via ferroelectricity. This aspect is demonstrated quantitatively in bilayer phosphorene at the doping concentration of $2.16 \times 10^{14}/\mathrm{cm}^2$, both states I and II possess the spin polarization energy of 12.69 meV/hole and magnetic moment of 1 μ_B/hole, while the distribution of magnetic moment is exchanged (i.e., 46% on the lower layer and 54% on the upper layer for state I; 54% on the lower layer and 46% on the upper layer for state II). Therefore, bilayer phosphorene and arsenene offer a fantastic platform for developing multifunctional multiferroic devices, such as information storage devices endowed with "efficient electrical writing and low-cost magnetic reading."

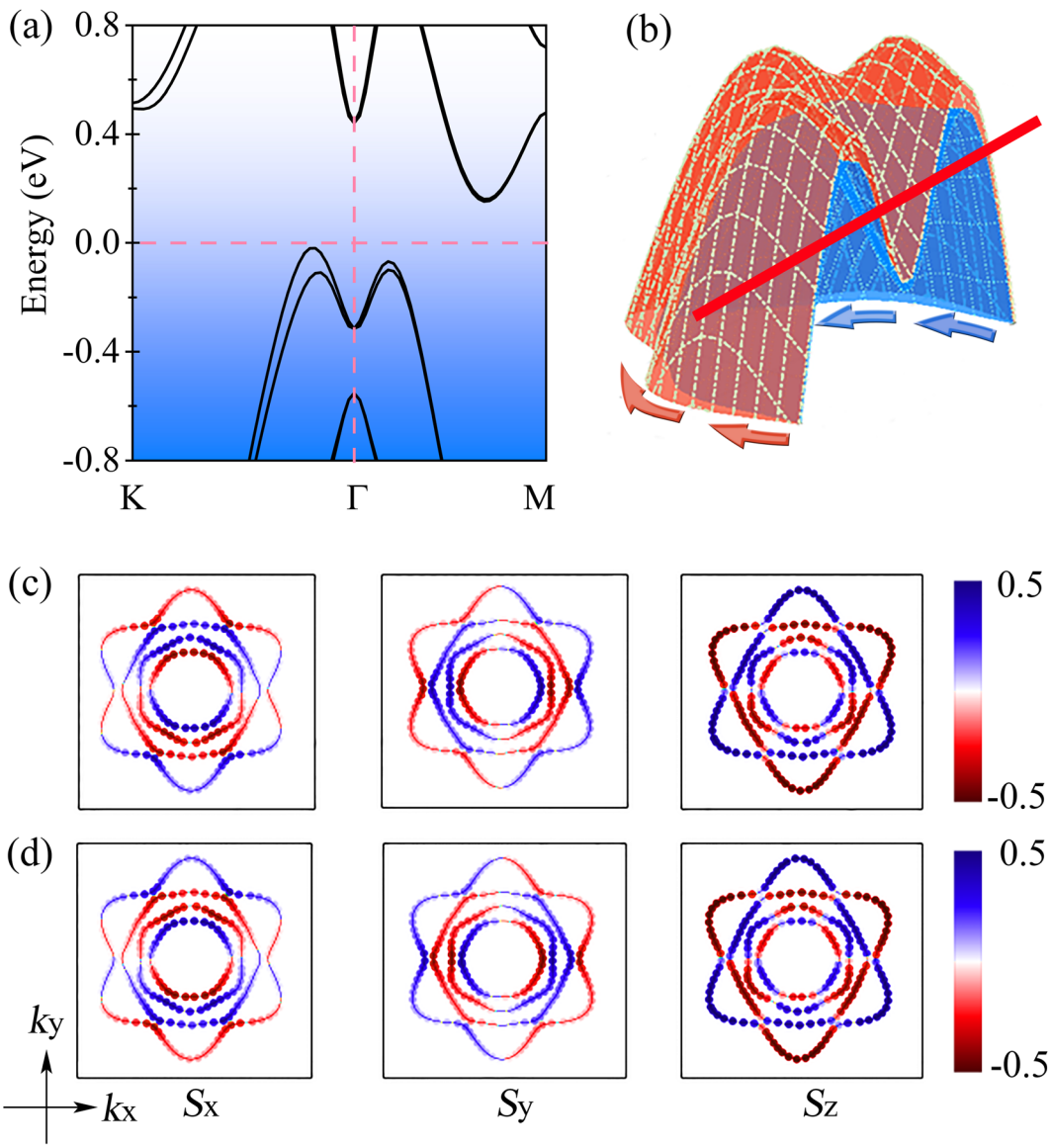

FIG. 5. (a) Band structure of bilayer antimonene with SOC. (b) 3D plot of the two highest valence bands near the Γ point for bilayer antimonene with SOC. The red line in (b) denotes the 2D cut plane for the energy surface (0.18 eV below the Fermi level), and the arrows refer to the in-plane spin orientation of outer and inner bands in bilayer antimonene under state I. Spin textures at the energy surface of 0.18 eV below the Fermi level for bilayer antimonene under (c) state I and (d) state II.

As centrosymmetry is broken for all these three systems, the Rashba effect can be expected in them. Band structures of bilayer antimonene, phosphorene, and arsenene with spin–orbit coupling (SOC) are included in Figs. 5(a) and S7. By comparing with the band structures shown in Figs. 5(a) and S7(c), we can see that the spin degeneracy for the highest valence band around the Γ point is lifted after considering SOC, producing an obvious Rashba splitting. This endows these systems being of great prospect for spintronic applications.

The coexistence of Rashba spin splitting and ferroelectricity in these systems makes us wonder whether it is possible to manipulate the spin of the electron via ferroelectricity. In the following, taking bilayer antimonene as an example, we prove that this is indeed accessible. Figures 5(c) and 5(d) show the spin textures at the energy surface of 0.18 eV below the Fermi level [Fig. 5(b)] for bilayer antimonene under states I and II. It can be seen that the in-plane spin components of the inner and outer bands rotate in opposite directions. For bilayer antimonene under state I [Fig. 5(c)], the in-plane spin direction of the inner (outer) surface band is counterclockwise (clockwise). The orientation of in-plane spin polarization is vividly depicted in Fig. 5(b). When switching the polarization direction of bilayer antimonene from $-z$ to $+z$ triggered by an external electric field, a reversal of in-plane spin textures occurs, see Fig. 5(d). Distinct from in-plane spin textures, OOP spin texture remains intact upon the inversion of OOP polarization. This discrepancy is sought into the fact that the spin precession of electrons experiences an effective magnetic field $\boldsymbol{B} = (\boldsymbol{p} \times \boldsymbol{E}/2mc^2)$.[23] The OOP spin is related to the in-plane dipole moment, which keeps unchanged when switching from state I to II. The in-plane spin is related to the OOP dipole moment, which is reversed when reversing the ferroelectric state. With these analyses in hand, we can easily understand this discrepancy. The ferroelectric control of spin textures can also be achieved in bilayer phosphorene and arsenene (Fig. S9). As a consequence, the close relationship between spin helicity and ferroelectric polarization is well established, providing a guidance for designing controllable spintronics.

In summary, we report the theoretical discovery of OOP ferroelectricity in 2D elemental materials, bilayer phosphorene, arsenene, and antimonene. These systems possess intriguing ferroelectricity with a sizeable OOP polarization, which originates from the charge redistribution induced by unique lattice stacking. Particularly, under hole doping, bilayer phosphorene and arsenene transform into the multiferroic phases, wherein the ferroelectricity and ferromagnetism are coupled strongly. Moreover, the spin textures for all these three systems can be engineered effectively via ferroelectric switching. These fascinating phenomena predicted in these elemental ferroelectric materials call for further experimental efforts.

See the supplementary material for the results of the phonon spectrum, *ab initio* molecular dynamic simulations, plane averaged electrostatic potentials, double-well profiles, pyroelectric responses, detailed band structures, and spin textures.

This work was supported by the National Natural Science Foundation of China (No. 11804190), Shandong Provincial Natural Science Foundation of China (Nos. ZR2019QA011 and ZR2019MEM013), Shandong Provincial Key Research and Development Program (Major Scientific and Technological Innovation Project) (No. 2019JZZY010302), Shandong Provincial Key Research and Development Program (No. 2019RKE27004), Qilu Young Scholar Program of Shandong University, and Taishan Scholar Program of Shandong Province.

DATA AVAILABILITY

The data that support the findings of this study are available within this article and its supplementary material.

REFERENCES

[1]J. H. Haeni, P. Irvin, W. Chang, R. Uecker, P. Reiche, Y. L. Li, S. Choudhury, W. Tian, M. E. Hawley, B. Craigo, A. K. Tagantsev, X. Q. Pan, S. K. Streiffer, L. Q. Chen, S. W. Kirchoefer, J. Levy, and D. G. Schlom, Nature **430**, 758 (2004).
[2]J. Valasek, Phys. Rev. **17**, 475 (1921).
[3]R. E. Cohen, Nature **358**, 136 (1992).
[4]Z. Peng, Y. Chen, Q. Chen, N. Li, X. Zhao, C. Kou, D. Xiao, and J. Zhu, J. Alloys Compd. **590**, 210–214 (2014).
[5]T. Ikeda and G. Yasuda, Jpn. J. Appl. Phys., Part 1 **14**, 1287 (1975).
[6]X. Moya, S. Kar-Narayan, and N. D. Mathur, Nat. Mater. **13**, 439 (2014).
[7]H. Wang, Z. R. Liu, H. Y. Yoong, T. R. Paudel, J. X. Xiao, R. Guo, W. N. Lin, P. Yang, J. Wang, G. M. Chow, T. Venkatesan, E. Y. Tsymbal, H. Tian, and J. S. Chen, Nat. Commun. **9**, 3319 (2018).
[8]P. Ghosez and K. M. Rabe, Appl. Phys. Lett. **76**, 2767 (2000).
[9]H. Kohlstedt, N. A. Pertsev, and R. Waser, MRS Proc. **688**, C6.5.1 (2001).
[10]J. Junquera and P. Ghosez, Nature **422**, 506 (2003).
[11]D. D. Fong, G. B. Stephenson, S. K. Streiffer, J. A. Eastman, O. Auciello, P. H. Fuoss, and C. Thompson, Science **304**, 1650 (2004).
[12]A. Munkholm, S. K. Streiffer, M. V. Ramana Murty, J. A. Eastman, C. Thompson, O. Auciello, L. Thompson, J. F. Moore, and G. B. Stephenson, Phys. Rev. Lett. **88**(1), 016101 (2001).
[13]M. Dawber, K. M. Rabe, and J. F. Scott, Rev. Mod. Phys. **77**, 1083 (2005).
[14]S. Yuan, X. Luo, H. L. Chan, C. Xiao, Y. Dai, M. Xie, and J. Hao, Nat. Commun. **10**, 1775 (2019).
[15]Z. Fei, W. Zhao, T. A. Palomaki, B. Sun, M. K. Miller, Z. Zhao, J. Yan, X. Xu, and D. H. Cobden, Nature **560**, 336 (2018).
[16]W. Ding, J. Zhu, Z. Wang, Y. Gao, D. Xiao, Y. Gu, Z. Zhang, and W. Zhu, Nat. Commun. **8**, 14956 (2017).
[17]R.-R. Ma, D.-D. Xu, Z. Guan, X. Deng, F. Yue, R. Huang, Y. Chen, N. Zhong, P.-H. Xiang, and C.-G. Duan, Appl. Phys. Lett. **117**, 131102 (2020).
[18]A. Chandrasekaran, A. Mishra, and A. K. Singh, Nano Lett. **17**, 3290 (2017).
[19]L. Li and M. Wu, ACS Nano **11**, 6382 (2017).
[20]T. Xu, J. Zhang, Y. Zhu, J. Wang, T. Shimada, T. Kitamura, and T. Y. Zhang, Nanoscale Horiz. **5**, 1400 (2020).
[21]J. Shang, C. Li, X. Tang, A. Du, T. Liao, Y. Gu, Y. Ma, L. Kou, and C. Chen, Nanoscale **12**, 14847 (2020).
[22]E. Bruyer, D. Di Sante, P. Barone, A. Stroppa, M.-H. Whangbo, and S. Picozzi, Phys. Rev. B **94**, 195402 (2016).
[23]Z. Lin, C. Si, S. Duan, C. Wang, and W. Duan, Phys. Rev. B **100**, 15548 (2019).
[24]S. Zhang, Z. Yan, Y. Li, Z. Chen, and H. Zeng, Angew. Chem., Int. Ed. **54**, 3112 (2015).
[25]C. Xiao, F. Wang, S. A. Yang, Y. Lu, Y. Feng, and S. Zhang, Adv. Funct. Mater. **28**, 1707383 (2018).
[26]Y. Wang, C. Xiao, M. Chen, C. Hua, J. Zou, C. Wu, J. Jiang, S. A. Yang, Y. Lu, and W. Ji, Mater. Horiz. **5**, 521 (2018).
[27]Z. Zhu, X. Cai, S. Yi, J. Chen, Y. Dai, C. Niu, Z. Guo, M. Xie, F. Liu, J.-H. Cho, Y. Jia, and Z. Zhang, Phys. Rev. Lett. **119**(10), 106101 (2017).
[28]D. Wang, L.-M. Tang, X.-X. Jiang, J.-Y. Tan, M.-D. He, X.-J. Wang, and K.-Q. Chen, Adv. Electron. Mater. **5**, 1800475 (2019).
[29]M. Wu, H. Fu, L. Zhou, K. Yao, and X. C. Zeng, Nano Lett. **15**, 3557 (2015).
[30]G. Kresse and J. Furthmüller, Phys. Rev. B **54**, 11169 (1996).
[31]J. P. Perdew, K. Burke, and M. Ernzerhof, Phys. Rev. Lett. **77**, 3865 (1996).
[32]S. Grimme, S. Ehrlich, and L. Goerigk, J. Comput. Chem. **32**, 1456 (2011).
[33]A. Togo and I. Tanaka, Scr. Mater. **108**, 1 (2015).
[34]G. Henkelman, B. P. Uberuaga, and H. Jónsson, J. Chem. Phys. **113**, 9901 (2000).

[35]N. R. Finney, M. Yankowitz, L. Muraleetharan, K. Watanabe, T. Taniguchi, C. R. Dean, and J. Hone, Nat. Nanotechnol. **14**, 1029 (2019).
[36]Z. Zhang, Y. Wang, K. Watanabe, T. Taniguchi, K. Ueno, E. Tutuc, and B. J. LeRoy, Nat. Phys. **16**, 1093 (2020).
[37]L. Bengtsson, Phys. Rev. B **59**, 12301 (1999).
[38]Q. Yang, M. Wu, and J. Li, J. Phys. Chem. Lett. **9**, 7160 (2018).
[39]X. Liu, Y. Yang, T. Hu, G. Zhao, C. Chen, and W. Ren, Nanoscale **11**, 18575 (2019).
[40]X. Jiang, Y. Feng, K. Q. Chen, and L. M. Tang, J. Phys. **32**, 105501 (2020).
[41]L. Kou, H. Fu, Y. Ma, B. Yan, T. Liao, A. Du, and C. Chen, Phys. Rev. B **97**, 075429 (2018).
[42]C. Liu, S. Guan, H. Yin, W. Wan, Y. Wang, and Y. Zhang, Appl. Phys. Lett. **115**, 252904 (2019).
[43]A. D. Bruce, Adv. Phys. **29**, 111 (1980).
[44]M. Wu, Z. Zhang, and X. C. Zeng, Appl. Phys. Lett. **97**, 093109 (2010).
[45]E. C. Stoner, Proc. R. Soc. A **154**, 656 (1936).
[46]L. J. Li, E. C. T. O'Farrell, K. P. Loh, G. Eda, B. Özyilmaz, and A. H. Castro Neto, Nature **529**, 185 (2016).
[47]T. Kolodiazhnyi, M. Tachibana, H. Kawaji, J. Hwang, and E. Takayama-Muromachi, Phys. Rev. Lett. **104**, 147602 (2010).
[48]Y. Shi, Y. Guo, X. Wang, A. J. Princep, D. Khalyavin, P. Manuel, Y. Michiue, A. Sato, K. Tsuda, S. Yu, M. Arai, Y. Shirako, M. Akaogi, N. Wang, K. Yamaura, and A. T. Boothroyd, Nat. Mater. **12**, 1024 (2013).
[49]X.-Y. Ma, H.-Y. Lyu, K.-R. Hao, Y.-M. Zhao, X. Qian, Q.-B. Yan, and G. Su, Sci. Bull. (published online).
[50]W. Luo, K. Xu, and H. Xiang, Phys. Rev. B **96**, 235415 (2017).